

## Article

# The Consequences of Dimension Reduction for Open Graded Friction Course (OGFC) Asphalt Mixtures: Morphological Characteristics and Finite Element Model (FEM) Simulation

Kai Li <sup>1</sup>, Quan Liu <sup>2,\*</sup>, Yuan Tian <sup>1</sup>, Cong Du <sup>1,\*</sup> and Zhixiang Xu <sup>3</sup><sup>1</sup> School of Qilu Transportation, Shandong University, Jinan 250016, China<sup>2</sup> College of Civil and Transportation Engineering, Hohai University, Nanjing 210098, China<sup>3</sup> PowerChina HuaDong Engineering Corporation Limited, Hangzhou 311122, China; xu\_zx5@hdec.com

\* Correspondence: quan.liu@hhu.edu.cn (Q.L.); congdu@sdu.edu.cn (C.D.)

**Abstract:** Asphalt mixtures exhibit complex mechanical behaviors due to their multiphase internal structures. To provide better characterizations of asphalt pavements under various forms of potential distress, a two-dimensional (2D) finite element simulation based on images of asphalt mixtures can be used to increase computational efficiency and reduce labor consumption. Nonetheless, using a representative image to eliminate the influence of dimension reduction from three dimensions to two dimensions is of great significance for attaining a reliable simulation result. Therefore, in this study, we investigated the consequence of dimension reduction for open-graded asphalt mixtures (denoted as OGFC-16), including a comprehensive characterization of these 2D models in terms of their morphologies and the similarities between them. This study aimed to reveal the variation in a 2D finite element simulation when applied to open-graded asphalt mixtures. Structural compositions, gradations, the aspect ratios of aggregates, and aggregate orientations were counted and calculated. In addition, the cosine similarity and structural similarity index measure (SSIM) were also calculated. Consequently, we performed a statistical analysis on the aforementioned indicators to quantitatively identify the discrepancy in the 2D images caused by dimension reduction. The results demonstrate that this 2D simulation might not be sufficient for representing the realistic mechanical performance of asphalt mixtures due to the remarkable variations in the image morphologies in different 2D images. However, the basic rules of stress behavior within structures can be accurately simulated. A compensative methodology for conducting a 2D simulation of open-graded asphalt mixtures should be based on a morphological characterization, considering structural compositions and the structural similarity index measure.

**Keywords:** finite element modeling; image discrepancy; morphological characteristics; indirect tensile test; image selection



**Citation:** Li, K.; Liu, Q.; Tian, Y.; Du, C.; Xu, Z. The Consequences of Dimension Reduction for Open Graded Friction Course (OGFC) Asphalt Mixtures: Morphological Characteristics and Finite Element Model (FEM) Simulation. *Buildings* **2024**, *14*, 545. <https://doi.org/10.3390/buildings14020545>

Academic Editor: Rui Xiao

Received: 14 December 2023

Revised: 8 February 2024

Accepted: 11 February 2024

Published: 18 February 2024



**Copyright:** © 2024 by the authors. Licensee MDPI, Basel, Switzerland. This article is an open access article distributed under the terms and conditions of the Creative Commons Attribution (CC BY) license (<https://creativecommons.org/licenses/by/4.0/>).

## 1. Introduction

During their service period, asphalt pavements are subject to various potential distresses, such as rutting deformation, moisture damage, and fatigue cracking [1]. These distresses are caused by varying inductions at different scales. Hence, it is vital to characterize asphalt mixtures from multi-scale perspectives to efficiently eliminate relative distresses. At the macro scale, also known as the global scale, critical pavement responses have been identified under the mechanistic–empirical pavement framework. To date, the most popular method of pavement design adopts finite element calculation to examine the mechanical responses of entire pavement structures. In terms of the mesoscale (also known as the local scale), asphalt mixtures are regarded as multi-phase composite materials. Approached from this aspect, cracking mechanisms and the stiffness contribution from each component can be well characterized in detail. Some research interests such as bitumen–aggregate

adhesion, bitumen diffusion, and bitumen modification require a better understanding of the asphalt mixtures at the micro scale.

Cross-scale research has always been an arduous challenge for highway researchers, particularly in the field of finite element simulation. In finite element modeling on a global scale, pavement is usually deemed a homogenous material in order to reduce computational costs. Previous studies demonstrated that simplification would not significantly affect simulation accuracy only if it was employed under proper mesh treatment [2,3]. On a local scale, two approaches are feasible for constructing an asphalt mixture model, depending on the simulation's purpose. One method is identical to that conducted on the global scale, in which a geometry model of asphalt mixtures is established with homogenous materials. Wang et al. used the extended finite element method to simulate a semi-circle bending (SCB) test. In their study, 3D SCB samples were modeled in ABAQUS, regarding the asphalt mixtures as isotropic and homogenous [4]. In addition, damage and fracture mechanical methods, such as the viscoelastic continuum damage (VECD) approach, were taken into account to investigate the fundamental mechanism behind the propagation of cracks within asphaltic materials [5]. Moreover, numerous efforts have been made towards deeply investigating crack initiations and propagations in asphalt pavements [6–8]. These studies provide a comprehensive outlook on the damage behavior of asphaltic materials and greatly facilitate research on improving the performance of asphalt pavements. However, the methods above failed to characterize micro-damage behavior, only accounting for the entire mechanical response. Alternatively, the asphalt matrix, aggregates, and air voids can be separately defined in one model to achieve a more precise simulation. Two methodologies are employed to construct microstructural models of asphalt mixtures; they are known as the random generation method and digital-image-processing (DIP) technology, respectively.

The random generation method develops a microstructural model with randomly distributed aggregates and air voids through a computer program, allowing for a great deal of labor to be efficiently reduced [9–11]. However, the random generation method fails to capture the natural characteristics of asphalt mixtures produced in the laboratory, likely generating unreliable simulation results. The introduction of DIP technology helps to construct more realistic microstructural models of asphalt mixtures. By far, the combination of DIP technology and the finite element (FE) method has been successfully adopted in many cases. Aiming to characterize the fracture-associated responses of asphalt mixtures, Rami et al. proposed a computational two-dimensional (2D) FE microstructural model [12]. Similarly, Coleri et al. demonstrated the feasibility of using two-dimensional (2D) and three-dimensional (3-D) FE models to predict the shear modulus values of asphalt mixtures [13]. Huang et al. also adopted the image-based finite element approach to study the rheological and mechanical responses of asphalt mixtures [14]. Liu et al. compared the mechanical responses of asphalt mixtures using different compaction methods via the 2D finite element method [15]. Kollmann et al. [16] adopted an optimized 2D microstructural FE model to explore the microstructural fracture behavior of asphalt mixtures. Sun et al. combined the local scale and global scale to analyze load-induced top-down cracking initiation in asphalt pavements [17]. It can be concluded from the above that, concerning the computational cost and technical efforts, most researchers prefer to use a two-dimensional-image finite element model to study the mechanical responses of asphalt mixtures.

On the other hand, it should be noted that, once the simulation scale is reduced to the local scale, damage initiation is usually ascribed to the presence of stress concentration, indicating an asphalt mixture's heterogeneity [18]. Therefore, the morphology of the 2D images used for finite element modeling is of great importance, likely governing the revelation of some decisive conclusions. Hence, selecting a representative 2D image plays a critical role in reasonable finite element modeling. Zhao et al. [19] noticed this issue and investigated two-dimensional finite element modelling for AC-type asphalt mixtures. It was concluded that aggregate content can be a critical indicator for the image selection process, aiming to improve calculation efficiency and accuracy. Compared with the AC-type

mixture, open-graded asphalt mixtures, owing to their discontinuous aggregate gradation, show more distinct structural variation. Therefore, aggregate content is not a sufficient indicator for the image selection process.

The finite element method has undoubtedly made significant contributions to the investigation of asphalt mechanical performance. However, it is crucial to emphasize that the 2D finite element model fails to accurately represent the actual microstructural characteristics of asphalt mixtures, potentially leading to a deviation in simulation accuracy. Therefore, this study focused on the simulation accuracy of open-graded asphalt mixtures in the case of two-dimensional simulation. For this reason, ten different 2D finite element models for open-graded asphalt mixtures were systematically characterized. Enlightened by the work conducted by Zhao et al. [19], similar analyses were carried out. In practice, the 2D models for open-graded asphalt mixtures showed significant variation concerning the mixtures' morphological characteristics. Hence, this study did not present a large number of 2D models, as the ten models already revealed the essential differences between these models. On the other hand, this study presents considerable work on the characterization of morphological characteristics, including regarding structural compositions, gradations, the aspect ratios of aggregates and aggregate orientations, cosine similarity, and the structural similarity index measure (SSIM). Finite element simulation was performed to calculate the indirect tensile strength (ITS) and indirect tensile modulus (ITSM). The entire structure of this manuscript is displayed in Figure 1.

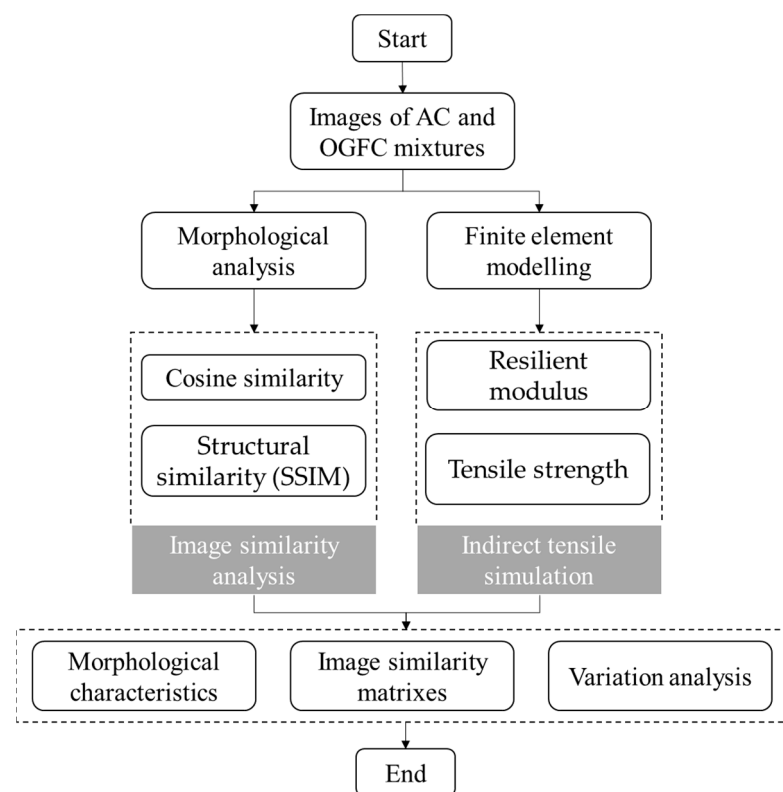


**Figure 1.** Flow chart of this study.

## 2. Characterization of 2D Models

### 2.1. Morphological Analysis of 2D Models

Ten 2D images of open-graded asphalt mixtures with a maximum nominal particle size of 16 mm (OGFC-16) were sourced from computed tomography (CT) scanning. In what follows, the morphological characteristics of aggregates and air voids are considered. All aggregates and air voids were identified with respect to their positions at constructed coordinates, as shown in Figure 2. The distance of each element to the center of a specimen was denoted as  $r$ . The area of each element was calculated in pixel units. An element's

orientation refers to the angle between the long axis of the fitting ellipse and the y-axis. The Feret diameter is defined as the distance between two parallel planes constraining an object perpendicular to the direction in question. The minimum and maximum diameters were derived through calculating each element's aspect ratio using Equation (1).

$$\text{Aspect ratio} = \frac{\text{Max. Feret diameter}}{\text{Min. Feret diameter}} \quad (1)$$

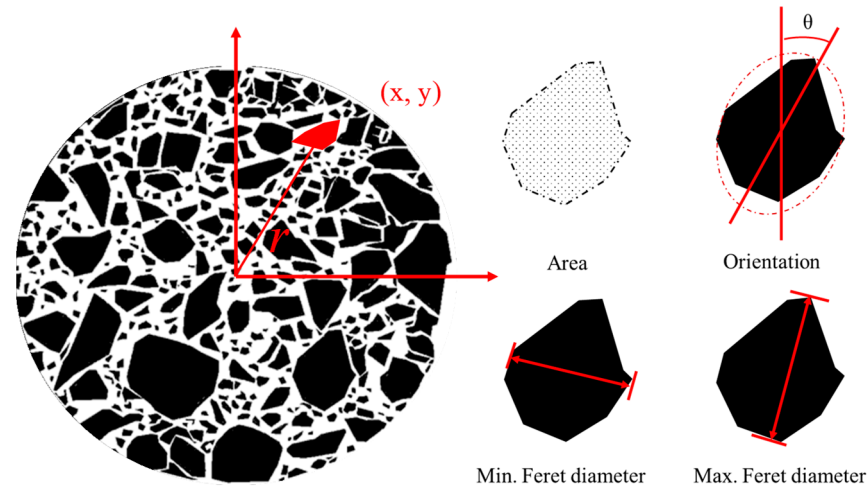


**Figure 2.** Schematic of image characterization.

In addition to primary indicators, we further characterized the images in terms of component fractions, particle area distribution, aspect ratio, and orientation distribution. Furthermore, two indicators were calculated based on the counted angles for aggregates, namely, the average orientation angle ( $\theta$ ) and the vector magnitude ( $\Delta$ ), as follows [20,21]:

$$\theta = \frac{\sum_{i=1}^N |\theta_i|}{N} \quad (2)$$

$$\Delta = \frac{100}{N} \sqrt{(\sum \sin 2\theta_i)^2 + (\sum \cos 2\theta_i)^2} \quad (3)$$

where  $N$  is the particle number, and  $\theta_i$  is the particle orientation angle.

In our quantitative analysis, we used the coefficient of variation (CoV) to describe image variation. In probability theory and statistics, the coefficient of variation is a measure of probability or frequency distribution. It is often expressed as a percentage and defined as the ratio of the standard deviation to the mean value, as expressed in Equation (4) [1].

$$\text{CoV} = \frac{\sigma}{\mu} \times 100\% \quad (4)$$

Here,  $\sigma$  represents the standard deviation, and  $\mu$  is the mean value.

## 2.2. Image Similarity Estimation among Different 2D Models

### 2.2.1. Cosine Similarity of Images

Cosine similarity is used to measure the similarity between two vectors, a quality defined in the following equations:

$$\text{Similarity} = \cos(\theta) = \frac{\mathbf{A} \cdot \mathbf{B}}{\|\mathbf{A}\| \|\mathbf{B}\|} = \frac{\sum_{i=1}^n A_i \times B_i}{\sqrt{\sum_{i=1}^n (A_i)^2} \times \sqrt{\sum_{i=1}^n (B_i)^2}} \quad (5)$$

where  $A_i$  and  $B_i$  represent the components of vectors  $\mathbf{A}$  and  $\mathbf{B}$ , respectively.

Before using cosine similarity to evaluate image similarity, the images were transformed to the vector format, followed by a cosine calculation conducted between two vectors. The whole calculation process was completed using MATLAB.

### 2.2.2. Structural Similarity Index Measure (SSIM)

The structural similarity index measure (SSIM) is another widely used method for estimating the similarity between two images. Structural similarity was defined using the following equation:

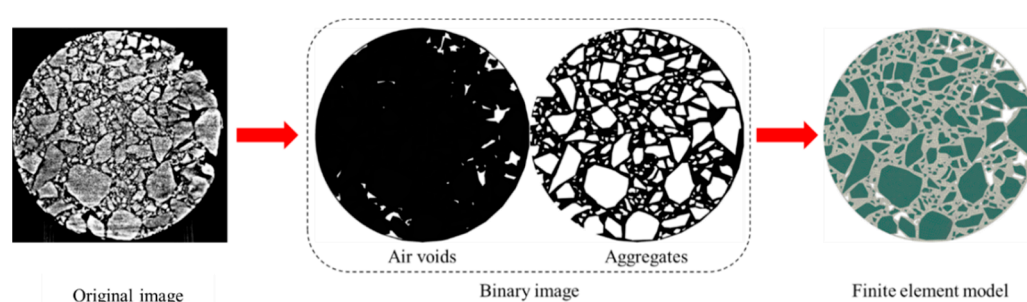
$$SSIM(x, y) = [l(x, y)]^\alpha [c(x, y)]^\beta [s(x, y)]^\gamma \quad (6)$$

where  $l$ ,  $c$ , and  $s$  represent the comparative measurements of luminance, contrast, and structure between two images, respectively.  $\alpha$ ,  $\beta$ , and  $\gamma$  are the weight parameters concerning the importance of  $l$ ,  $c$ , and  $s$ , respectively. In this calculation, the weight parameters used for  $\alpha$ ,  $\beta$ , and  $\gamma$  were 0, 0, and 1, respectively.

## 3. Finite Element Modeling of 2D Images

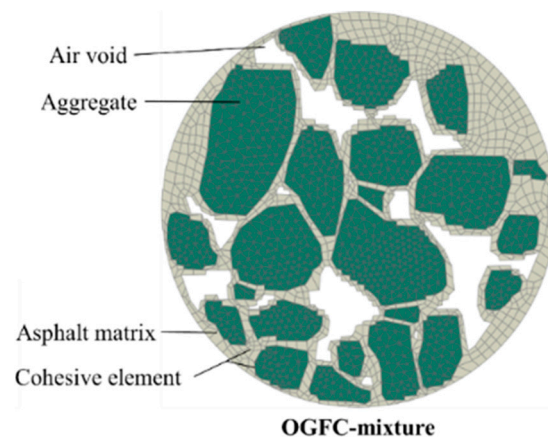
### 3.1. Model Construction Using Digital Image Processing (DIP)

Figure 3 illustrates the modelling process from the original image to the 2D microstructure model developed via FEM. Original X-ray CT images of asphalt mixtures were first converted into binary images based on the grayscale of the images in MATLAB. The binary images provided essential information on the internal structures of the asphalt mixtures, including regarding aggregate particles and air voids. Afterwards, the outlines of the aggregates and air voids were extracted using a polygonal approximation algorithm, whereby the internal structures of the asphalt mixtures were transformed into coordinates. Therefore, these coordinates were input into Abaqus software (version Abaqus/CAE 2017) to develop 2D models of the asphalt mixture using a Python (version 2.7.3) pre-processor [22]. Subsequently, the images were transferred into 2D FEM models. As a result of this process, the aggregate resolution critically influenced precision and efficiency; aggregates smaller than 2.36 mm were removed from the model. On the other hand, the mesh size is supposed to account for computational duration and accuracy simultaneously. For this reason, a preliminary mesh study was performed to determine the mesh size, considering the models' complexities, computation time, computation convergences, and computational precision. Consequently, the global mesh size for the OGFC-type mixture was 2.5 mm.



**Figure 3.** Images depicting the application of digital image processing (DIP) to the CT images.

In addition to asphalt compositions, the zero-thickness cohesive element was incorporated in the model to simulate asphalt mixtures' cracking behavior. Cohesive elements were inserted among asphalt matrix elements as well as matrix–aggregate interfaces. In this case, micro cracks can randomly generate and propagate along the boundaries of aggregates and within the asphalt matrix. The constructed FEM models for OGFC-16 are shown in Figure 4.



**Figure 4.** Image of element distribution within the microstructure model.

### 3.2. Constitutive Models Used for Simulation

Constitutive models and specific parameters are listed in Table 1. The Young's modulus and Poisson's ratio of the aggregates were 55,000 MPa and 0.2, respectively. Linear viscoelastic constitutive relation in the form of the Prony series was used to describe the asphalt matrix, as shown in Equation (7) [17]:

$$E = E_e + \sum_{i=1}^N E_i e^{-t/\rho_i} \quad (7)$$

where  $E_e$  is the equilibrium modulus; the set of  $[\rho_i, E_i]$  ( $i = 1, 2, \dots, N$ ) is the discrete relaxation spectrum.

**Table 1.** Model parameters of the 2D simulation of asphalt mixtures.

Bilinear Cohesive Zone Model			$t^0 = 3 \text{ MPa}, G = 2.75 \text{ kJ/m}^2$		
Prony Series with $\mu = 0.35$					
$i$	$\rho_i$ (s)	$E_i$ (MPa)	$i$	$\rho_i$ (s)	$E_i$ (MPa)
1	$1.00 \times 10^{-7}$	5218.14	8	$1.00 \times 10^0$	512.63
2	$1.00 \times 10^{-6}$	5381.72	9	$1.00 \times 10^1$	154.93
3	$1.00 \times 10^{-5}$	5499.81	10	$1.00 \times 10^2$	55.72
4	$1.00 \times 10^{-4}$	5570.35	11	$1.00 \times 10^3$	13.97
5	$1.00 \times 10^{-3}$	5112.13	12	$1.00 \times 10^4$	6.79
6	$1.00 \times 10^{-2}$	3608.49	$E_e$	-	34.20
7	$1.00 \times 10^{-1}$	1489.17			

Crack propagation was described by the cohesive zone model (CZM) [23]. Figure 5 presents a schematic of the CZM model. In accordance with previous studies, the bilinear traction–separation law (TSL) was used to characterize the cracking behavior of asphalt mixtures [17,23,24]. The bilinear TSL is determined by three parameters, including traction strength  $t_0$ , separation displacement  $\delta_{sep}$ , and fracture energy  $G$ . The following quadratic nominal stress damage criterion was employed to initiate cracking [17]:

$$G_n = \frac{1}{2} t_n^0 \delta_n^{sep} \quad (8)$$

$$G_t = \frac{1}{2} t_t^0 \delta_t^{sep} \quad (9)$$

where the subscripts  $n$  and  $t$  refer to the normal and tangential components, respectively.

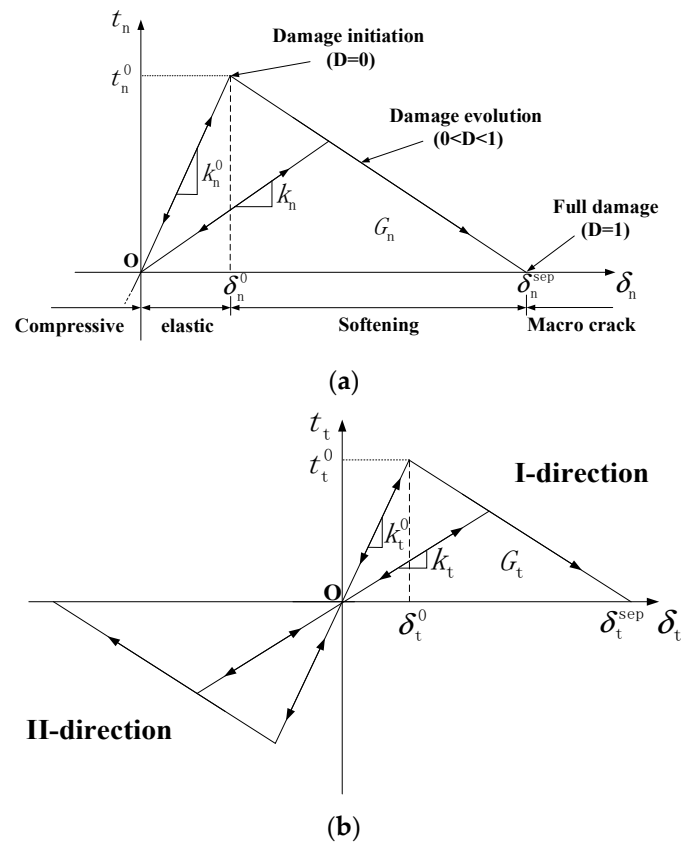


**Figure 5.** Image of the bilinear traction–separation law (TSL) [25]: (a) normal component; (b) tangential component.

### 3.3. Simulation of an Indirect Tensile Test

An indirect tensile test was simulated in compliance with AASHTO TP31-96 [26]. The environmental temperature and loading rate for simulating the two asphalt mixtures were set to be identical: 20 °C and 50 mm/min, respectively. According to the simulation results, the indirect tensile resilient modulus and the indirect tensile strength can be calculated using the following equations [26]:

$$S_T = \frac{P_T \times (0.27 + \mu)}{h \times X_T} \quad (10)$$

$$R_T = 0.006287P_T/h \quad (11)$$

where  $S_T$  is the indirect tensile resilient modulus (MPa);  $R_T$  is indirect tensile strength (MPa);  $P_T$  is the amplitude of the applied load (N);  $\mu$  is Poisson's ratio;  $X_T$  is the amplitude of the horizontal strain (mm); and  $h$  is the height of the specimen (mm), which was set as 40 mm in this study.

## 4. Results and Discussion

### 4.1. Morphological Characteristics of 2D Images

Asphalt mixtures are composed of an aggregate skeleton, a bitumen matrix, and air voids. The mechanical performance of asphalt mixtures is associated with the air void ratio, aggregate gradation, aggregate angularity, and microstructures after compaction. Accordingly, our morphological analysis of the 2D images focused on the phase compositions, particle size distribution, aspect ratios of aggregates and air voids, and the orientations of aggregates and air voids. It is worth noting that the calculated parameters might vary with respect to those in real asphalt mixtures due to dimension reduction.

#### 4.1.1. Phase Compositions

Figure 6 shows the counted phase components for the OGFC asphalt mixtures. It can be seen that the aggregate fraction varied from 35% to 55%, indicating a broad range of aggregate content. The aggregate structure contributes to the strength formation of asphalt mixtures. Therefore, it can be deduced that the significant variation in aggregate content would undoubtedly cause a simulation difference, provided that 2D images were used rather than three-dimensional models. Concerning air voids, the OGFC asphalt mixture is that with an air void above 15%, according to the corresponding definition [27]. However, the calculated air void based on the 2D image was smaller than the actual value (decreasing from 6% to 13%). Therefore, reducing an image from 3D to 2D could induce an unavoidable error in calculation, and this fact was considered in advance. In both cases of aggregate or air void fractions, two primary compositions with a significant variation were detected, indicating that the use of 2D images in finite element modelling might induce a loss of structural information.

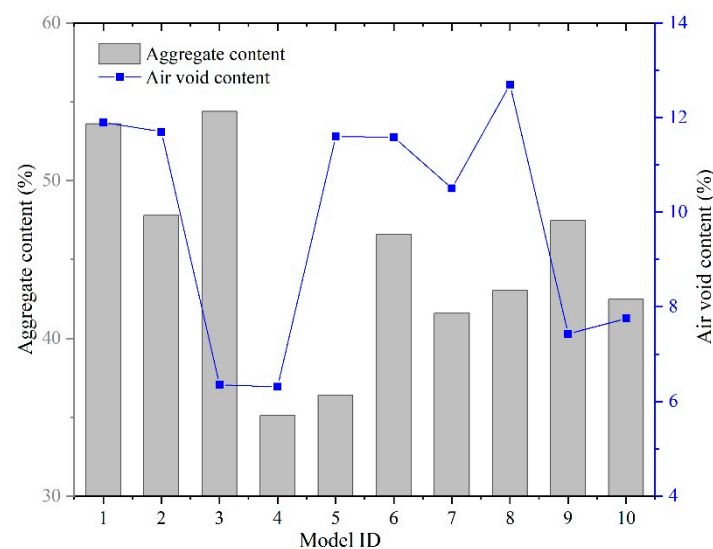


**Figure 6.** Component fractions of aggregates and air voids for OGFC.

#### 4.1.2. Particle Area Distribution

Apart from the phase composition, aggregate gradation is another critical factor that affects the mechanical performance of asphalt mixtures. In a 2D image, the particle area distribution can indirectly reflect the particle size distribution. Also, it should be noticed here that the counted particle area distribution deviated from the actual distribution due to dimension reduction. However, the variation in the counted ten images is the primary concern of this study. Figure 7 presents the particle area distribution, including aggregate and air void components.

It can be seen that the particle area distribution of aggregates exhibited differences; however, the basic shapes for the distribution curve were consistent, excluding images I8 and I1. Nevertheless, the maximum particle area showed significant variation, as shown in the positions at an accumulative passing percentage of 100%. The maximum particle area for image I4 was around  $0.5 \times 10^4$ , while in the case of image I1, this value reached  $1.3 \times 10^4$ .

As for the air voids, a consistent particle area distribution for most images can be observed. Also, two exceptions were found, as seen in images I3 and I8. Accordingly, one should be cautious when using images I1, I3, and I8 to model asphalt mixtures.

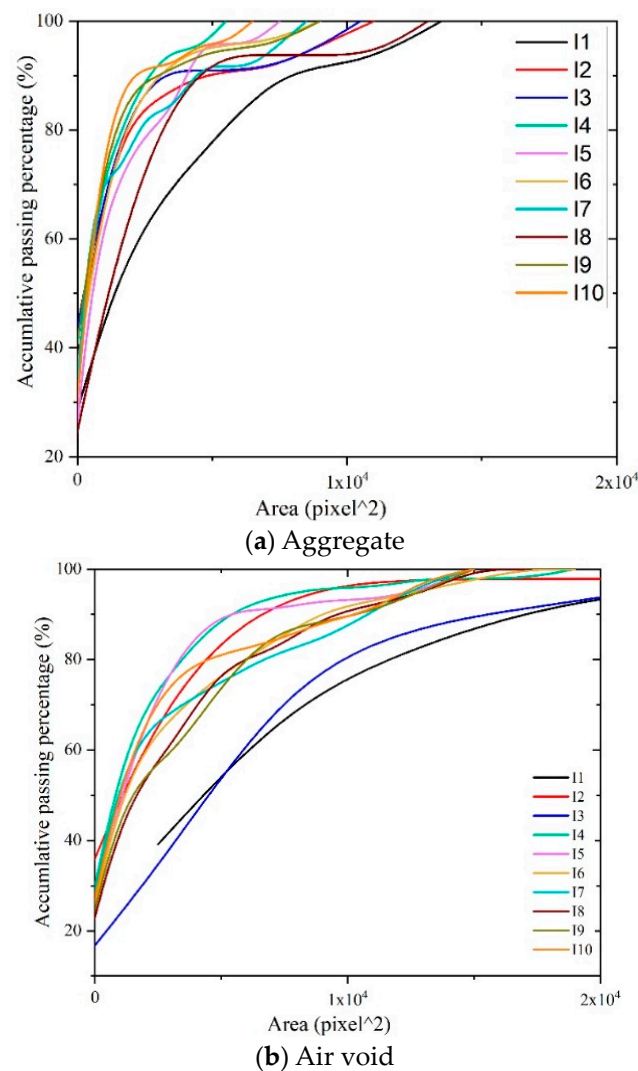


**Figure 7.** Particle area distribution of OGFC: (a) aggregate; (b) air void.

#### 4.1.3. Aspect Ratio

Another factor influencing the mechanical performance of asphalt mixtures is the angularity of coarse aggregates characterized by the aspect ratio of the aggregates. Therefore, in this study, we calculated the aspect ratio of each aggregate in 2D images and the aspect ratios of formed air voids. Statistical analysis of the counted aspect ratio was carried out, as shown in Figure 8.

The ten investigated images showed an identical aspect ratio distribution with the medium value fluctuating between 1.5 and 2.0. Because the aspect ratio is not related to the compaction process, the stable values of different images indicated a relatively homogenous distribution of coarse aggregates. However, concerning the aspect ratio of the air void, the variation was significant. For example, in image I3, the aspect ratio shows a broad distribution and is higher than the others. This illustrates that the air voids that formed in I3 tended to be flat, while in other cases, the air voids tended to be very round. Different from the aspect ratio of aggregates, the air voids were formed in the compaction process. Therefore, the medium value of the aspect ratio of the aggregates showed more significant variation than the air voids.

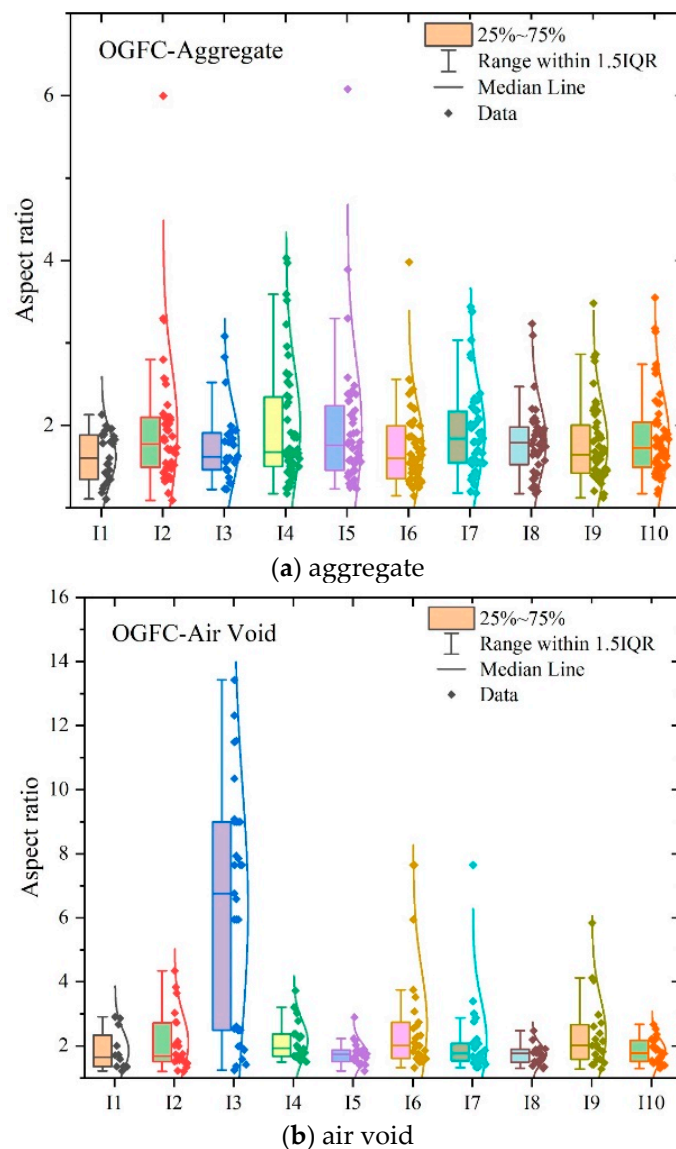


**Figure 8.** Aspect ratio distribution of OGFC asphalt mixtures: (a) aggregates; (b) air voids.

#### 4.1.4. Summary of Our Morphological Analysis of the 2D Images

Table 2 shows the calculated coefficients of variation for different indicators. It can be seen that the  $CoV$  varied from 1.74% to 68.12%. Some concerning indicators presented stability with a low  $CoV$ , such as the aspect ratio of aggregates ( $ASRA$ ) at 5.99%, and the aggregate fraction ( $AF$ ) was 7.4%. On the other hand, the  $CoV$  of the  $ASRAV$  reached 68.12%, and the air void fraction ( $AVF$ ) was 46.3%. The  $CoVs$  of the average orientation angles ( $\theta$ ) of the aggregates, denoted as  $\theta(A)$ , and the vector magnitudes ( $\Delta$ ) of the aggregates, denoted as  $\Delta(A)$ , were 7.22% and 5.91%, respectively. Almost all the  $CoVs$  were constrained within 10%, which is an acceptable level in most practical engineering scenarios. It was indicated that the average orientation angle and vector magnitude would not significantly change due to the dimension reduction from 3D to 2D. Concerning the average orientation angle ( $\theta$ ) of the air voids, denoted as  $\theta(AV)$ , the  $CoV$  was 11%. However, regarding the vector magnitude ( $\Delta$ ) of the air voids, denoted as  $\Delta(AV)$ , the  $CoV$  reached 16.31%. This large  $CoV$  could be ascribed to a limited amount of air void, thus tending toward a large variation coefficient.

**Table 2.** Coefficient-of-variation analysis for concerning indicators.

	<i>AF</i>	<i>CoV</i>	<i>AVF</i>	<i>CoV</i>	<i>ASRA</i>	<i>CoV</i>	<i>ASRAV</i>	<i>CoV</i>
1	53.72		2.85		1.62		1.84	
2	53.4		5.84		1.95		2.09	
3	60		1.22		1.76		8.05 *	
4	56.67		2.07		1.98		2.17	
5	57.7	7.4%	2.29	46.3%	1.95	6.0%	1.75	68.1%
6	53.8		1.98		1.74		2.66	(14.1% *)
7	50.28		2.05		1.92		2.15	
8	58.4		3.8		1.81		1.74	
9	45.6		2.27		1.77		2.37	
10	55.6		2.25		1.86		1.84	
	$\theta (A)$	<i>CoV</i>	$\theta (AV)$	<i>CoV</i>	$\Delta (A)$	<i>CoV</i>	$\Delta (AV)$	<i>CoV</i>
1	39.59		50.32		54.32		47.00	
2	49.26		48.69		53.04		57.06	
3	46.96		61.99		62.27		76.38	
4	46.22		48.21		54.85		41.12	
5	42.43	7.2%	51.38	11.0%	63.06	5.9%	61.84	16.3%
6	50.04		45.1		60.66		60.81	
7	48.96		46.56		55.97		54.04	
8	44.78		43.67		61.62		59.40	
9	41.86		51.14		58.65		56.12	
10	44.88		41.57		60.29		48.83	

$\theta (A)$ : Average orientation angle of aggregates.  $\theta (AV)$ : Average orientation angle of an air void.  $\Delta (A)$ : Vector magnitude of aggregates.  $\Delta (AV)$ : Vector magnitude of an air void. \* The value 14.1% was calculated by removing the data 8.05.

The morphological analysis of the 2D images of the OGFC asphalt mixtures revealed that, due to the dimension reduction from 3D to 2D, the 2D-based finite element modeling method might not be adaptable. Based on the comparison made in this study, several preliminary conclusions can be inferred regarding morphological characteristics: (1) The reduction in dimensions from 3D to 2D leads to a loss of crucial structural information, particularly regarding composition and pore structures. Consequently, this results in the distortion of simulated mechanical properties. (2) Morphological features associated with the original source, such as aggregates, remain relatively unchanged. Hence, the variations in *AF*, *ASRA*,  $\theta (A)$ , and  $\Delta (A)$  fall within an acceptable range (within 10%). However, significant disparities exist in the features formed during the compaction process, which introduces uncertainty into the simulated mechanical properties.

#### 4.2. Image Similarity Matrixes

The abovementioned indicators are conventional parameters used to evaluate image morphology. However, these indicators can vary due to the accuracy of image segmentation and recognition. This section discusses the possibility of an overall comparison that includes all the model information between two models, for which an analysis of image similarity was attempted. Specifically, the cosine similarity and structural similarity index measure were calculated.

Figure 9 presents the similarity matrices for the ten images studied. It can be seen that using cosine similarity to measure image similarity resulted in a higher similarity degree compared with such degrees calculated using the SSIM. It can be intuitively seen that, according to both cosine similarity and the SSIM, the highest similarity degree was observed between images I1 and I3. Images I2 and I6 had the lowest similarity for both methods.

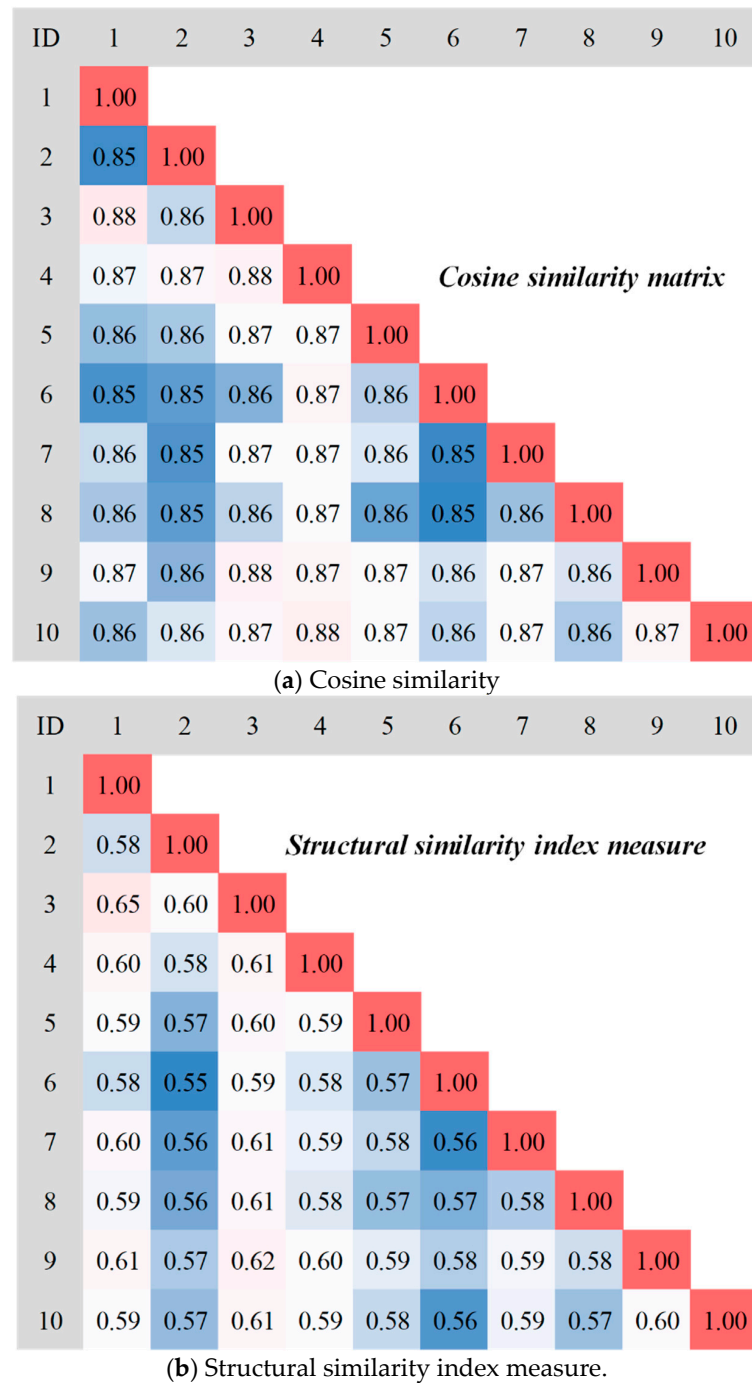


**Figure 9.** Image similarity matrix: (a) cosine similarity; (b) SSIM.

On the other hand, the similarity determined via cosine similarity ranged from 0.85 to 0.88, while the similarity based on the SSIM ranged from 0.55 to 0.65. Through comparison, it can be found that the SSIM was superior to cosine similarity with respect to identifying image differences. Therefore, we selected the SSIM as the similarity measure for the ten images investigated.

#### 4.3. Variation Analysis Based on 2D FE Simulation Results

This section shows the finite element simulation results for the ten 2D images above. On the one hand, the variation analysis of the simulated indirect tensile strength and indirect tensile modulus demonstrated that the dimension reduction could affect the

simulation reliability. On the other hand, the stress distribution pattern of the simulation results provided a visual evaluation of image variation.

#### 4.3.1. Stress Distribution Pattern

The horizontal stress distributions simulated for the different images are presented in Figure 10. Most of the images showed identical stress distribution patterns, which can be expressed as follows. Stress concentration primarily occurred along the loading axis. Tensile stress was observed in the asphalt matrix, while aggregates bore the compression stress. However, the stress distribution patterns for I1 and I5 were different. Significantly, stress concentration was not observed. This might have been due to the presence of a large air void near the loading point. As a result, the targeted deformation was easily achieved on account of the compression of the air void. Therefore, the actual applied stress for I1 and I5 was relatively lower than that of the other images. This indicates that the distribution of air voids remarkably affected the simulation results. In addition, 2D images with large air voids near the loading point are not recommended for simulation.

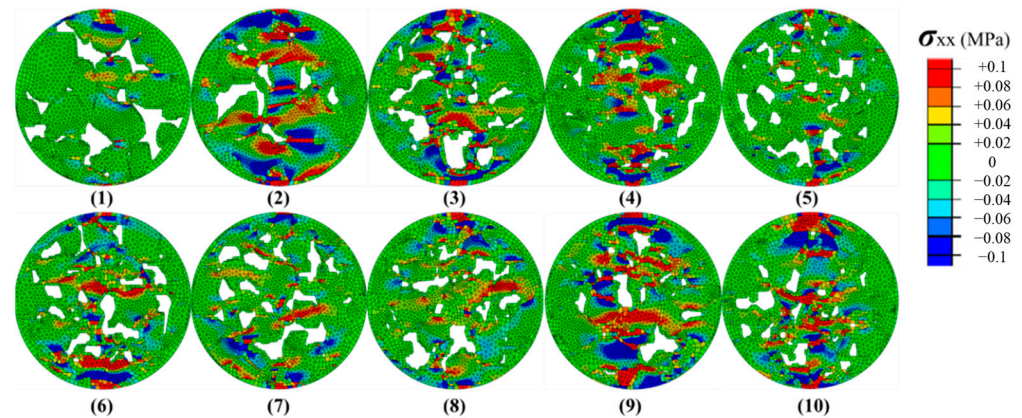
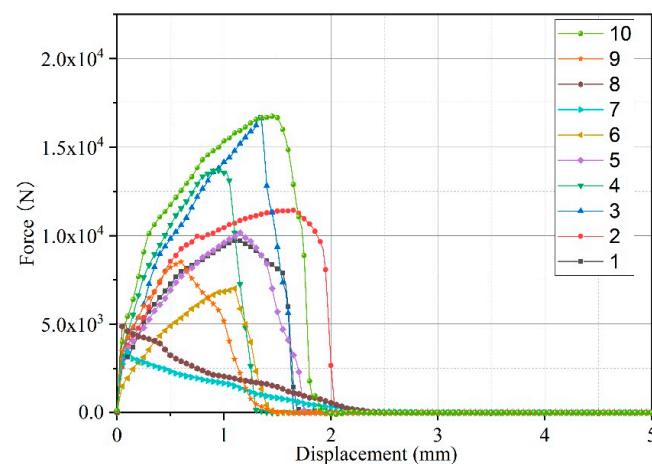


Figure 10. Images of stress distribution.

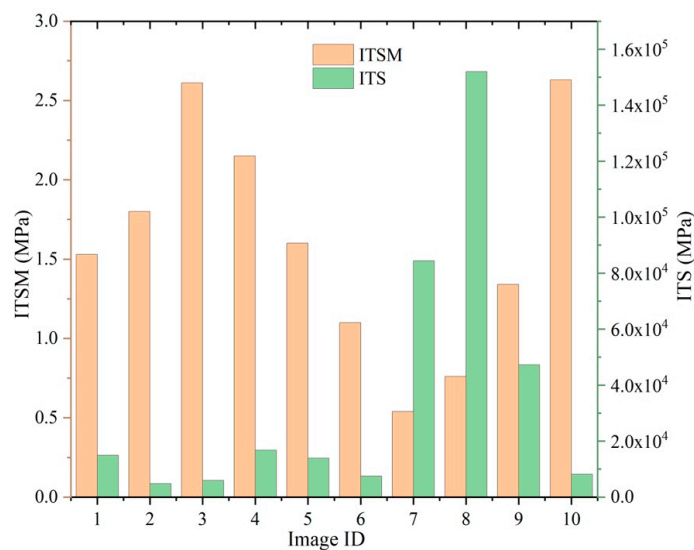
#### 4.3.2. Force–Strain Curves

Force–strain curves derived from indirect tensile strength simulation were also investigated, as shown in Figure 11. The simulated force–strain curves of I7 and I8 were peculiar: as shown, the peak values could be reached with a small strain applied. This finding can be ascribed to the same phenomenon discussed for the stress distribution pattern.



(a)

Figure 11. Cont.



(b)

**Figure 11.** Indirect tensile strength simulation results: (a) Force–displacement curve; (b) *CoV* results.

## 5. Conclusions

The research in this article reveals significant disparities in the microstructure and simulation outcomes of asphalt mixtures, particularly for the OGFC type, when employing two-dimensional finite element modeling. This highlights the necessity of carefully considering the representativeness of 2D models while investigating asphalt mixtures using the two-dimensional finite element method. This study examined OGFC asphalt mixtures from both morphological characteristics and simulation result perspectives, leading to the following key findings.

The morphologies of the 2D images, although sourced from the same asphalt mixtures, showed remarkable variations in the mixture compositions and aggregate gradations. In addition, morphological characteristics such as aspect ratio were not significantly altered. By comparing ten 2D finite element results, it was found that 2D simulation might not represent the actual mechanical responses of asphalt mixtures due to the dimension reduction from 3D to 2D. However, the stress pattern exhibits reasonable stress transformations in structures, constituting the key properties of asphalt mixtures for withstanding external loads. Hence, it is still meaningful to use 2D finite element simulations to identify the basic rules of material properties.

This study revealed the consequences of dimension reduction from 3D to 2D in the finite element modelling of asphalt mixtures in terms of morphological characteristics and simulation results. However, 3D models of the two asphalt mixtures could not be developed due to a lack of three-dimensional information. Hence, the three-dimensional mechanical behavior of asphalt mixtures remains unknown, and the relationship between the 3D and 2D simulation results was unclear. To this end, further work should be focused on preparing asphalt mixture samples in a laboratory and developing 2D and 3D models for finite element simulations. Consequently, deep insight into the mechanical characterizations yielded by 2D and 3D models can be developed, and reasonable methods for aiding the selection of the optimal 2D image when modelling asphalt mixtures can be proposed.

**Author Contributions:** Conceptualization, C.D. and Q.L.; methodology, K.L.; software, Z.X.; validation, C.D., K.L. and Y.T.; formal analysis, C.D.; investigation, Q.L.; resources, C.D.; data curation, Z.X.; writing—original draft preparation, K.L.; writing—review and editing, C.D.; visualization, Q.L.; project administration, C.D.; funding acquisition, C.D. and Y.T. All authors have read and agreed to the published version of the manuscript.

**Funding:** This research was funded by the Natural Science Foundation of Jiangsu Province, grant number BK20230256.

**Data Availability Statement:** Date will be available on request.

**Conflicts of Interest:** The authors declare no conflicts of interest.

## References

1. Wu, J.; Liu, Q.; Wang, Y.; Chen, J.; Wang, D.; Xie, L.; Ago, C. Effect of Mixing Time and Temperature on the Homogeneity of Asphalt Mixtures Containing Reclaimed Asphalt Pavement Material. *Transp. Res. Rec.* **2018**, *2672*, 167–177. [\[CrossRef\]](#)
2. Liu, P.; Xing, Q.; Wang, D.; Oeser, M. Application of Linear Viscoelastic Properties in Semianalytical Finite Element Method with Recursive Time Integration to Analyze Asphalt Pavement Structure. *Adv. Civ. Eng.* **2018**, *2018*, 9045820. [\[CrossRef\]](#)
3. Ling, C.; Arshadi, A.; Bahia, H. Importance of binder modification type and aggregate structure on rutting resistance of asphalt mixtures using image-based multi-scale modelling. *Road Mater. Pavement Des.* **2017**, *18*, 785–799. [\[CrossRef\]](#)
4. Wang, X.; Zhang, J.; Li, K.; Ding, Y.; Geng, L. Cracking Analysis of Asphalt Mixture Using Semi-circle Bending Method. *Iran. J. Sci. Technol. Trans. Civ. Eng.* **2021**, *45*, 269–279. [\[CrossRef\]](#)
5. Board, T.R. *National Academies of Sciences, Engineering, and Medicine. Top-Down Cracking of Hot-Mix Asphalt Layers: Models for Initiation and Propagation*; The National Academies Press: Washington, DC, USA, 2010.
6. Ameri, M.; Mansourian, A.; Heidary Khavas, M.; Aliha, M.R.M.; Ayatollahi, M.R. Cracked asphalt pavement under traffic loading—A 3D finite element analysis. *Eng. Fract. Mech.* **2011**, *78*, 1817–1826. [\[CrossRef\]](#)
7. Wang, H.; Ozer, H.; Al-Qadi, I.L.; Duarte, C.A. Analysis of Near-Surface Cracking under Critical Loading Conditions Using Uncracked and Cracked Pavement Models. *J. Transp. Eng.* **2013**, *139*, 992–1000. [\[CrossRef\]](#)
8. Dinegdae, Y.H.; Birgisson, B. Effects of truck traffic on top-down fatigue cracking performance of flexible pavements using a new mechanics-based analysis framework. *Road Mater. Pavement Des.* **2018**, *19*, 182–200. [\[CrossRef\]](#)
9. Yin, A.; Yang, X.; Zhang, C.; Zeng, G.; Yang, Z. Three-dimensional heterogeneous fracture simulation of asphalt mixture under uniaxial tension with cohesive crack model. *Constr. Build. Mater.* **2015**, *76*, 103–117. [\[CrossRef\]](#)
10. Wang, H.; Wang, J.; Chen, J. Micromechanical analysis of asphalt mixture fracture with adhesive and cohesive failure. *Eng. Fract. Mech.* **2014**, *132*, 104–119. [\[CrossRef\]](#)
11. Yin, A.; Yang, X.; Gao, H.; Zhu, H. Tensile fracture simulation of random heterogeneous asphalt mixture with cohesive crack model. *Eng. Fract. Mech.* **2012**, *92*, 40–55. [\[CrossRef\]](#)
12. Rami, K.Z.; Amelian, S.; Kim, Y.-R.; You, T.; Little, D.N. Modeling the 3D fracture-associated behavior of viscoelastic asphalt mixtures using 2D microstructures. *Eng. Fract. Mech.* **2017**, *182*, 86–99. [\[CrossRef\]](#)
13. Coleri, E.; Harvey, J.T.; Yang, K.; Boone, J.M. Development of a micromechanical finite element model from computed tomography images for shear modulus simulation of asphalt mixtures. *Constr. Build. Mater.* **2012**, *30*, 783–793. [\[CrossRef\]](#)
14. Huang, W.; Wang, H.; Yin, Y.; Zhang, X.; Yuan, J. Microstructural Modeling of Rheological Mechanical Response for Asphalt Mixture Using an Image-Based Finite Element Approach. *Materials* **2019**, *12*, 2041. [\[CrossRef\]](#)
15. Liu, P.; Hu, J.; Wang, D.; Oeser, M.; Alber, S.; Ressel, W.; Canon Falla, G. Modelling and evaluation of aggregate morphology on asphalt compression behavior. *Constr. Build. Mater.* **2017**, *133*, 196–208. [\[CrossRef\]](#)
16. Kollmann, J.; Lu, G.; Liu, P.; Xing, Q.; Wang, D.; Oeser, M.; Leischner, S. Parameter optimisation of a 2D finite element model to investigate the microstructural fracture behaviour of asphalt mixtures. *Theor. Appl. Fract. Mech.* **2019**, *103*, 102319. [\[CrossRef\]](#)
17. Sun, Y.; Du, C.; Zhou, C.; Zhu, X.; Chen, J. Analysis of load-induced top-down cracking initiation in asphalt pavements using a two-dimensional microstructure-based multiscale finite element method. *Eng. Fract. Mech.* **2019**, *216*, 106497. [\[CrossRef\]](#)
18. Du, C.; Sun, Y.; Chen, J.; Gong, H.; Wei, X.; Zhang, Z. Analysis of cohesive and adhesive damage initiations of asphalt pavement using a microstructure-based finite element model. *Constr. Build. Mater.* **2020**, *261*, 119973. [\[CrossRef\]](#)
19. Zhao, Y.; Jiang, L.; Jiang, J.; Ni, F. Accuracy Improvement for Two-Dimensional Finite-Element Modeling while Considering Asphalt Mixture Meso-Structure Characteristics in Indirect Tensile Test Simulation. *J. Mater. Civ. Eng.* **2020**, *32*, 04020275. [\[CrossRef\]](#)
20. Masad, E.; Muhunthan, B.; Shashidhar, N.; Harman, T. Internal Structure Characterization of Asphalt Concrete Using Image Analysis. *J. Comput. Civ. Eng.* **1999**, *13*, 88–95. [\[CrossRef\]](#)
21. Hassan, N.; Airey, G.; Khan, R.; Collop, A. Nondestructive characterisation of the effect of asphalt mixture compaction on aggregate orientation and segregation using X-ray computed tomography. *Int. J. Pavement Res. Technol.* **2012**, *5*, 84–92.
22. Xing, C.; Xu, H.; Tan, Y.; Liu, X.; Zhou, C.; Scarpas, T. Gradation measurement of asphalt mixture by X-ray CT images and digital image processing methods. *Measurement* **2019**, *132*, 377–386. [\[CrossRef\]](#)
23. Zegeye Teshale, E. Low-Temperature Fracture Behavior of Asphalt Concrete in Semi-Circular Bend Test. Ph.D. Dissertation, University of Minnesota, Minneapolis, MN, USA, 2012.
24. Baek, J. Modeling Reflective Cracking Development in Hot-Mix Asphalt Overlays and Quantification of Control Techniques. Ph.D. Thesis, University of Illinois at Urbana-Champaign, Champaign, IL, USA, 2010.
25. Chakraborty, A.; Ghosh, S.; Mukhopadhyay, P.; Dinara, S.; Bag, A.; Mahata, M.; Kumar, R.; Das, S.; Jana, S.; Majumdar, S.; et al. Trapping Effect Analysis of AlGaIn/InGaIn/GaIn Heterostructure by Conductance-Frequency Measurement. In Proceedings of the MRS Fall Meeting 2015, Boston, MA, USA, 29 November–4 December 2015.

26. *ASTM D7369-11*; Standard Test Method for Determining the Resilient Modulus of Bituminous Mixtures by Indirect Tension Test. ASTM International: West Conshohocken, PA, USA, 2011.
27. Gu, F.; Watson, D.; Moore, J.; Tran, N. Evaluation of the benefits of open graded friction course: Case study. *Constr. Build. Mater.* **2018**, *189*, 131–143. [[CrossRef](#)]

**Disclaimer/Publisher’s Note:** The statements, opinions and data contained in all publications are solely those of the individual author(s) and contributor(s) and not of MDPI and/or the editor(s). MDPI and/or the editor(s) disclaim responsibility for any injury to people or property resulting from any ideas, methods, instructions or products referred to in the content.